

Chapter 2

Freestanding Silicene

Obtaining a freestanding 2D graphene flake is relatively easy because it has a naturally occurring 3D layered parent material, graphite, made up of graphene layers weakly bound to each other by van der Waals interaction. In fact, graphite is energetically more favorable than diamond (which is one of the most stable and hard materials on Earth) that is the sp^3 hybridized allotrope of carbon. To prepare freestanding graphene, it is enough to come up with a smart procedure for isolating the weakly bound layers of graphite. The same is also true for other layered materials like hexagonal boron nitride, black phosphorus, metal dichalcogenides and oxides. Silicene, on the other hand, doesn't have a naturally occurring 3D parent material since silicon atoms prefer sp^3 hybridization over sp^2 hybridization. This makes the synthesis of freestanding silicene very hard, if not impossible. However, it is possible to epitaxially grow silicene on metal substrates and make use of its intrinsic properties by transferring it to an insulating substrate (Tao et al. 2015). In this chapter, we focus on intrinsic properties of freestanding silicene in the absence of the metallic substrate.

2.1 Reconstructions of Bulk Silicon Surfaces

Synthesis of 2D crystal structures can be achieved through various experimental techniques such as chemical vapor deposition, micromechanical cleavage, liquid exfoliation and dry exfoliation. Whether it is grown on a surface or cleaved from bulk, the atomic structure of a natural 2D material resembles one of its crystallographic surfaces and planes. Therefore, to apprehend the formation and unique features of silicene, understanding the properties of various surfaces of bulk silicon is essential.

A surface can be described as the truncated form of the bulk material. In case of a crystal, the surface region is defined as the few outermost layers of the material. For covalently bonded crystals, when the truncation takes place, the presence of dangling bonds at the surface, that contain less than two spin-paired electrons, is inevitable at the surface. Due to the presence of such dangling bonds the structural, electronic and magnetic properties at the surface may become significantly different from those of the bulk material.

The space lattice of bulk silicon, which has a diamond structure, is face-centered cubic. In this structural arrangement, where each Si atom is tetrahedrally bonded to neighboring atoms, some crystallographic planes display quite different structural properties. Noteworthy, as seen in Fig. 2.1, especially the buckled hexagonal symmetry of the Si(111) surface exactly resembles the monolayer honeycomb lattice structure of silicene. The formation of a Si(111) surface is energetically the most favorable one. Since the Si(111) surface has the lowest density of dangling bonds, it has the lowest surface energy. Therefore, since formation of such a surface is favored over the other types of surfaces, the natural cleavage plane and growth direction of bulk Si can be expected to be [111] direction.

When a surface is formed, firstly surface atoms tend to change their atomic position inward or outward slightly a phenomenon called *surface relaxation*. Furthermore, the presence of dangling bonds at the surface results in an unstable atomic order and these atoms tend to change their position to find the lowest energy configuration. Such a structural transformation driven by the dangling hybrids is called *surface reconstruction*. As proposed by Jahn and Teller, if there is a degeneracy in the ground state of a molecular structure its atoms will re-arrange toward a lower symmetry (Jahn and Teller 1937). Such a structural-degeneracy-driven deformation is called a Jahn-Teller distortion. Similarly, upon the relaxation and reconstruction mechanisms, surface structure spontaneously releases its surface energy (or surface tension) by reducing the number of dangling bonds.

Since silicon devices are mostly grown on Si(100) substrates, revisiting its characteristic properties is of importance for silicene studies. At the (100) silicon plane each atom is bonded to two underlying atoms and therefore, one can expect

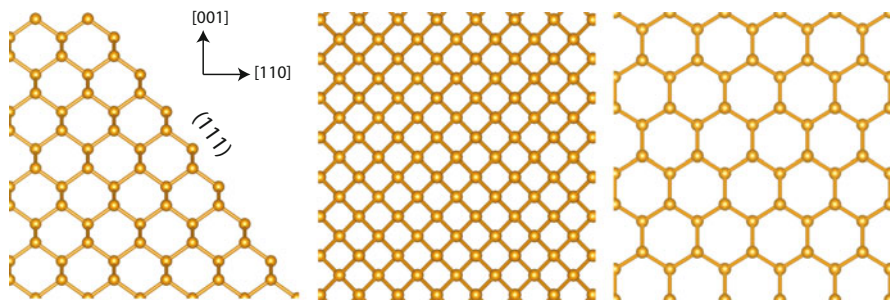


Fig. 2.1 (Left panel) View of unreconstructed surfaces of silicon through the $(1\bar{1}0)$ plane. Atomic arrangements at (110) and (111) surfaces are shown in the *mid* and *right* panels, respectively

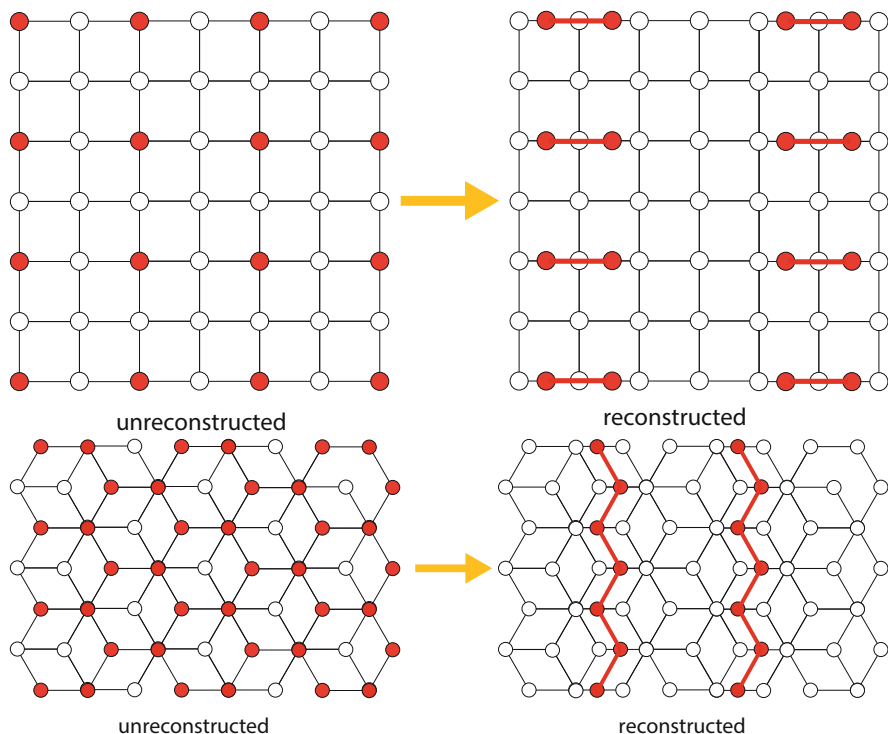


Fig. 2.2 *Top panels:* top views for the Si(100) unreconstructed and (2×1) reconstructed surfaces. Uppermost surface Si atoms are colored red. *Lower panels:* top views for the unreconstructed Si(111) surface and its (2×1) reconstruction. Atoms at uppermost two layers are represented by red balls

creation of two dangling hybrids upon the surface creation. Studies have shown that while the resulting surface has a 2×1 periodicity at room temperature (see Fig. 2.2), thanks to the diversity of arrangements of dangling hybrids the formation of this surface may take place in different ways (Phillips 1973; Poppendieck et al. 1978; Krüger and Pollmann 1995).

The Si(111) surface also form a 2×1 reconstruction upon in situ cleavage under ultra-high vacuum (Lander et al. 1963). In this configuration π -bonded chains of locally sp^2 -bonded atoms create one-dimensional Si chains at the surface, as initially proposed by Pandey (1981). Since Si(111)- (2×1) structure is irreversibly transformed into a 7×7 reconstruction at ~ 700 K, followed by a reversible $7 \times 7 \leftrightarrow 1 \times 1$ transition to a 1×1 structure at ~ 1100 K, it can be considered as a metastable phase of the surface.

The 7×7 reconstruction of the Si(111) surface, composed of 49 Si(111) primitive cells, is much more complex. Although it was first observed very early in a Low Energy Electron Diffraction (LEED) experiment (Schlier and Farnsworth 1959) due to the insufficiency of experimental characterization tools the atomic structure of

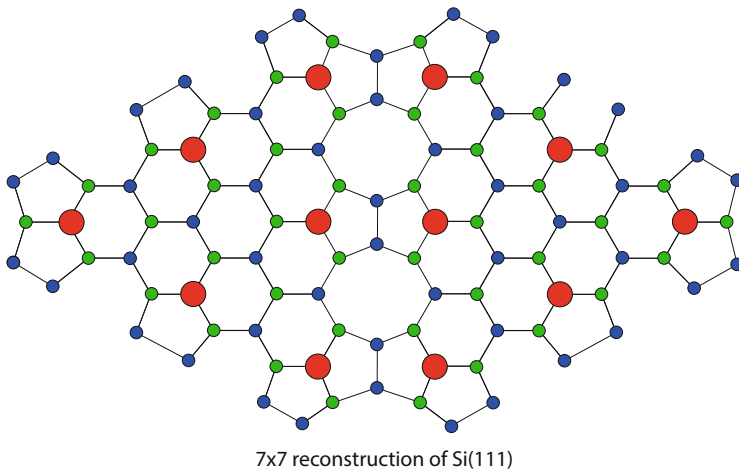


Fig. 2.3 Top view for the (7×7) reconstruction of the Si(111) surface. Adatoms, first-layer-atoms and second layer atoms are shown by red, green and blue balls, respectively

the surface was an intriguing open question for a long term. The determination of the complicated surface topology of the Si(111)-(7×7) surface was performed only in 1985 by Takayanagi et al., surprisingly by transmission electron diffraction using thinned Si(111) sample in an UHV microscope (Takayanagi et al. 1985).

As shown in Fig. 2.3, the 7×7 reconstruction takes place, according to the so-called *dimer adatom stacking-fault model*, by (1) formation of hole sites at each cell corner, (2) formation of pentagons, which are linked by the dimers at the second layer, in the middle of the 7×7 unitcell and (3) adsorption of 12 adatoms on this surface. Upon this reconstruction, the number of surface dangling bonds is reduced from 49 to 19 (12 for the adatoms, six for the so-called rest atoms and one for the atom in the center of the corner hole) per unitcell. Therefore, the energy of the unreconstructed Si(111) surface is significantly lowered through the 7×7 reconstruction.

These early studies clearly show that silicon, besides being the key material in semiconductor device technology possesses easy-to-reconstruct complex surfaces, which offer a rich playground for variety of electronic and physical properties.

2.2 Atomic Structure and Stability of Freestanding Silicene

If one searches for the silicon counterpart of graphene, a natural start would be to replace C atoms with Si and find the optimum lattice constant. A standard density functional theory (DFT) calculation (Kresse and Joubert 1999) performed using the projector-augmented wave (PAW) method (Blöchl 1994) and the PBE exchange-correlation functional (Perdew et al. 1996) results in a planar silicene with a lattice

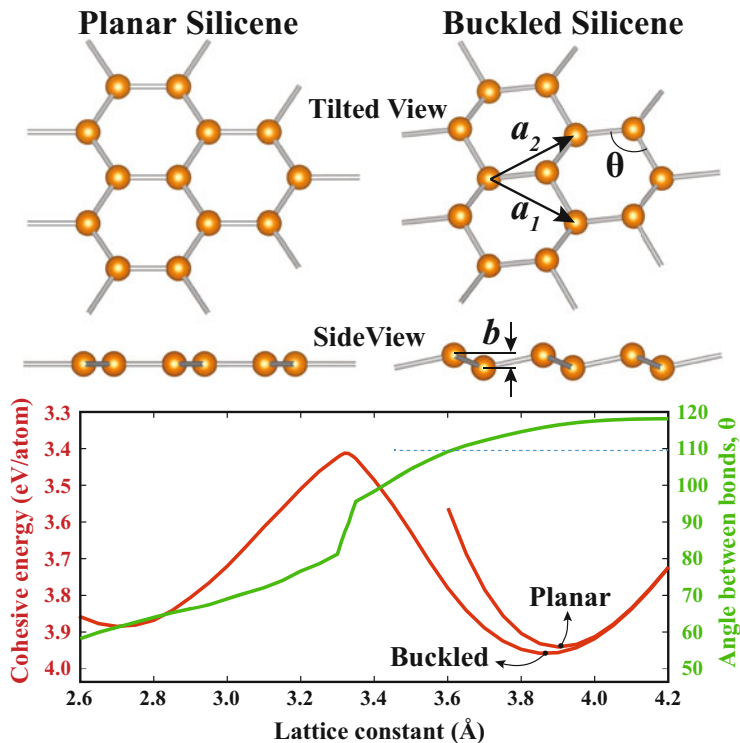


Fig. 2.4 The *top panel* shows ball and stick models of planar and buckled silicene from tilted and side views. The *bottom panel* shows the variations of the cohesive energy (red solid line) and bond angle (green solid line) with respect to the lattice constant. The thin dashed blue line represents the ideal bond angle of sp^3 hybridization

constant of 3.90 \AA . However, this optimum value is found only because one puts a constraint by confining Si atoms in a single plane. Once this constraint is removed, silicene goes to a more energetically favorable state that has a lattice constant of 3.87 \AA and a slight buckling of 0.45 \AA (see Fig. 2.4). There are two main reasons why this buckling occurs in silicene and not in graphene. First, Si atoms prefer sp^3 hybridization over sp^2 which pulls bond angles from 120° towards 109.5° . Second, the distance between Si atoms in silicene becomes rather large to maintain a strong π -bonding. Despite this, the hybridization of silicene is closer to sp^2 than to sp^3 . This can be quantified by making use of the fact that in the ideal cases the degree of hybridization, that is D of sp^D , is correlated with the ideal bond angles θ in such a way that $D = -1/\cos(\theta)$. This relation holds true for carbon allotropes like atomic chains, graphene and diamond that have sp , sp^2 and sp^3 hybridization with bond angles 180° , 120° and 109.5° , respectively. In the case of silicene, the bond angle is $\theta = 116.2^\circ$ which gives $D \sim 2.27$.

In Fig. 2.4 we present the variations of the cohesive energy and bond angle of silicene as the lattice constant is changed. The energy minima for planar and slightly buckled silicene are clearly seen. As the lattice constant is squeezed by $\sim 0.5 \text{ \AA}$, the system enters to a new regime. This is accompanied with a sudden change in the bond angle. A new energy minimum is found when the lattice constant is squeezed even further. However, the geometry of this new energy minimum is quite different from that of silicene. The bond angles almost approach 60° ; as a consequence, the second neighbor Si atom is almost as close as the first one which means that each Si atom has nine neighbors. It was shown that this unlikely structure is unstable (Cahangirov et al. 2009).

The buckled structure of silicene was first proposed by Takeda and Shiraishi in 1994 while the name silicene was coined by Guzmán-Verri and Lew Yan Voon in a 2007 publication that investigated the planar structure (Takeda and Shiraishi 1994; Guzmán-Verri and Lew Yan Voon 2007). However, silicene remained ignored until it was shown that the buckled structure was indeed thermodynamically stable (Cahangirov et al. 2009). This was achieved by calculation of vibrational modes for both planar and buckled silicene. While for planar silicene the phonon dispersion had imaginary frequencies in the buckled case all modes were positive over the whole Brillouin zone, indicating that there was a restoring force for all possible atomic displacements.

The phonon dispersions for planar and buckled silicene are shown in Fig. 2.5. The out of plane optical mode (ZO) of planar silicene has imaginary values at the Γ point indicating instability. This mode corresponds to displacement of Si atoms in one sublattice up and atoms in the other sublattice down along the axis passing

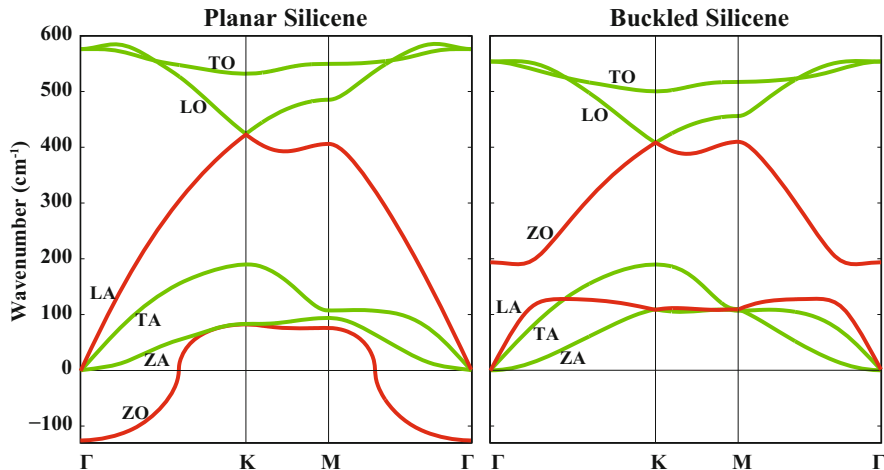


Fig. 2.5 Phonons of planar and buckled silicene. The out of plane, transverse and longitudinal acoustic and optical modes are denoted by ZA, TA, LA, ZO, TO and LO, respectively. The LA and ZO modes change significantly upon structural transformation. These modes are shown by *red lines* to call attention to this change

perpendicular to planar silicene. It means that if one tries to push atoms of planar silicene in this particular way, there will be no restoring force against it. When we go from planar to buckled silicene the LA and ZO modes change significantly while others remain almost the same. Upon buckling, the imaginary part of the ZO mode in planar silicene moves up to 200 cm^{-1} replacing the portion of the LA mode that was connected to the LO mode. Meanwhile, the positive portion of the ZO mode in planar silicene becomes a part of the new LA mode.

Note that the stability analysis presented here ignores many experimentally relevant effects like thermal fluctuations and reactivity. Suspended graphene sheets were shown to have ripples caused by thermal fluctuations that reach 1 nm in height (Meyer et al. 2007). A similar behavior is expected for silicene. However, due to its high reactivity, it is almost impossible to synthesize silicene in its freestanding form (Brumfiel 2013). Instead, growth of silicene requires the presence of a substrate that can stabilize its two-dimensional structure that is not the ground state of silicon. The sticky nature of silicene is also the reason why the layered allotrope of silicon, like graphite, doesn't exist in nature. All this is excellently expressed in the “silicene interlude” written by the 1981 Chemistry Nobel Prize Laureate Roald Hoffmann. He explains that in silicon chemistry, single σ -bonds are favored over double π -bonds and the latter need to be protected sterically in order to be isolated (Hoffmann 2013). For this reason, freestanding silicene will latch to any molecular dirt in its environment. Fully hydrogenated silicene or silicane, on the other hand, should be possible to synthesize in the freestanding form.

2.3 Electronic Structure of Freestanding Silicene

Although freestanding silicene is buckled, the hybridization in Si atoms remains closer to sp^2 rather than becoming sp^3 . In Fig. 2.6 we compare the electronic structure of planar and buckled silicene. When silicene is planar, the p_z orbitals do not mix with others. This is clearly seen in the linearly crossing bands at the K point that are solely composed of p_z orbitals. However, upon buckling, these states get a minor but noticeable contribution from both s and p_{xy} orbitals. Similarly, p_z bands cross s and p_{xy} bands near the Γ point in planar silicene while in buckled silicene this crossing splits and bands rehybridize. The electrons of buckled silicene behave as massless Dirac fermions due to the linearly crossing bands at the Fermi level. The Fermi velocity of these bands is around $0.53 \times 10^6\text{ m/s}$ when the LDA or PBE functionals are employed and increases to $0.68 \times 10^6\text{ m/s}$ when a hybrid functional like HSE06 is used (Drummond et al. 2012). This velocity is close to that of freestanding graphene which is experimentally measured to be around $1 \times 10^6\text{ m/s}$ (Novoselov et al. 2005).

Furthermore, silicene also has properties that are not found in graphene. Due to the buckled structure it is possible to tune the electronic properties of silicene by applying an electric field in the perpendicular direction (Drummond et al. 2012). The slope of the band gap with respect to the applied perpendicular electric field was

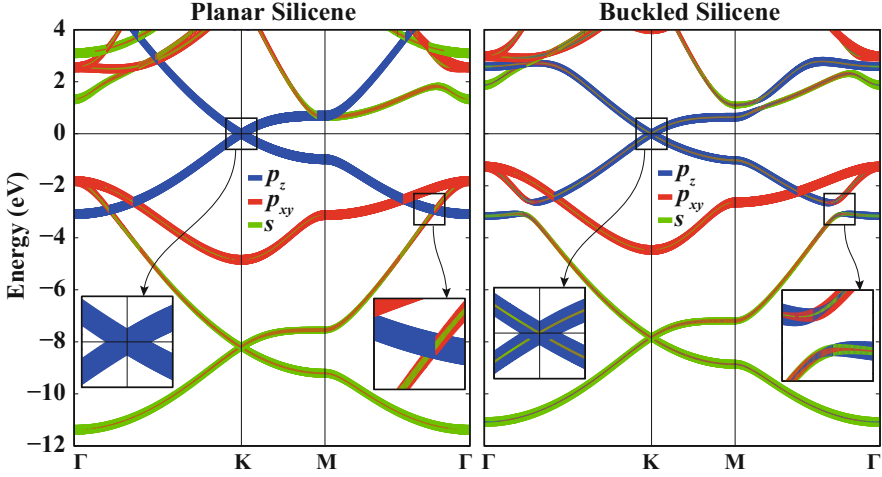


Fig. 2.6 The electronic structures of planar and buckled silicene. The orbital character of each state is shown by colors. The width of each line is proportional to the contribution from the orbital denoted by the color (blue, red, and green for p_z , p_{xy} and s orbitals, respectively) of that line. The orbital with lower contribution is plotted on top of the one that has higher contribution, which makes all contributions visible. Some parts of the bands are shown in more detail in the insets

found to be $\sim 0.07 \text{ e}\text{\AA}$. This value is eight times higher when it is estimated using first-order perturbation theory that does not include screening which suggests that silicene has strong sublattice polarizability. Owing to the larger spin-orbit coupling in Si compared to C, silicene has topologically non-trivial states with a spin-orbit gap of 1.5 meV (Liu et al. 2011; Drummond et al. 2012). The topological insulator state of silicene protects a gapless spectrum of edge states. When the perpendicular electric field reaches the critical value of 20 mV/\AA , silicene makes transition from the topological to a band insulator state (Drummond et al. 2012). These states are more pronounced in germanene and stanene as will be discussed in Chap. 5. Depending on the applied exchange field and perpendicular electric field, a broad range of phases emerge in silicene that include a quantum anomalous Hall insulator, a valley polarized metal, a marginal valley polarized metal, a quantum spin Hall insulator and a band insulator (Ezawa 2012).

2.4 Hydrogenation: Silicane and Germanane

Silicene not only provides an alternative monolayer to graphene but also prepares a ground for derivation of novel silicon-based functionalized materials. Rapidly growing experimental and theoretical research on graphene derivatives have shown that production of high quality functionalized crystals, each with different electronic

and magnetic properties, can be realized in many different ways (such as hydrogenation, fluorination, chlorination, oxygenation, defect patterning, strain application and adatom/molecule decoration). Thanks to the advances in functionalization techniques, novel silicene derivatives, which are promising to be integrated into a widespread collection of nanoscale optoelectronic devices, have emerged. Here we review how silicene can be functionalized and what are the characteristic properties of silicene-based functionalized materials.

Hydrogenation process is a chemical reaction of hydrogen molecule with a surface, molecule or an element. While most of the hydrogenation processes need presence of a metallic catalyst, non-catalytic hydrogenation can only take place at high temperatures. Alkenes are hydrocarbons with at least one double bond. However, reaction of the carbon-carbon double bond in an Alkene with hydrogen leads to formation of an Alkane. Alkanes are hydrocarbons with only single bonds between the carbon atoms. Following the terminology of chemistry one can name the conversion from graphene to fully hydrogenated graphene as conversion from graphene to graphane. As firstly predicted by Sofo et al., Graphane, a sp^3 hybridized hexagonal network of graphene hydrogenated on both sides of the plane in an alternating manner, is stable and its binding energy is comparable to other hydrocarbons such as benzene, cyclohexane, and polyethylene (Sofo et al. 2007). Graphane, with formula CH , has been reported as an insulator with nonmagnetic ground state. Following experimental efforts by Elias et al. graphane was synthesized by cold hydrogen plasma treatment of graphene (Elias et al. 2009). The characteristic insulating nature of graphane (with about 5 eV bandgap) and its possible use in nanodevice technologies have been well-documented in a review (Sahin et al. 2015).

It was shown that, the optical properties of graphane are dominated by the localized charge-transfer excitations governed by the enhanced electron correlations in a 2D dielectric medium (Cudazzo et al. 2010). The strong electron-hole interaction in graphane leads to the appearance of small radius bound excitons which open the path towards the possibility of excitonic Bose-Einstein condensation that might be observed experimentally. This can also be true for silicon and germanium counterparts of graphane discussed below (Fig. 2.7).

It is known that similar to graphene structural analogue of benzene can also be formed by silicon atoms (Barton and Burns 1978). However, differing from benzene rings silicon rings are stabilized in a chair-shaped atomic structure (Abersfelder et al. 2010). Therefore, the buckled geometry of monolayer silicene provides an ideal ground for hydrogen treatment of its surfaces. By adopting the terminology used for graphene, a one-by-one hydrogenation process turns silicene into silicane. In order to avoid the confusion between the names 'graphene' and 'graphane', generally graphane's name is written as "graphAne" in the literature. Similarly, one can make use of the same definition to name silicAne and germanAne, the fully-hydrogenated derivatives of silicene and germanene.

As shown in Fig. 2.8a, silicane which is analogous to graphane has a buckled honeycomb structure with a single hydrogen atom attached to each Si site on either sides of the 2D crystal. Voon et al., for the first time, studied the structural and

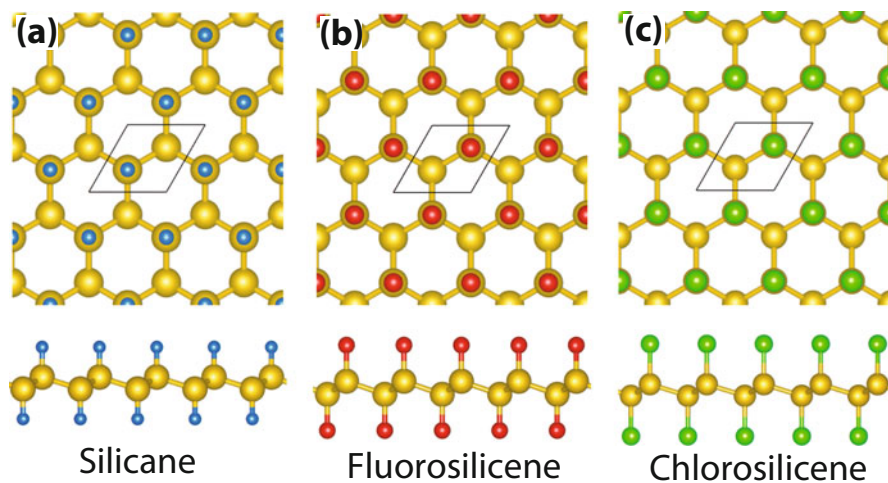


Fig. 2.7 Top and side views of the atomic structures of fully (a) hydrogenated, (b) fluorinated and (c) chlorinated silicene. Hydrogen, fluorine and chlorine atoms are represented by *blue, red and green* colors, respectively

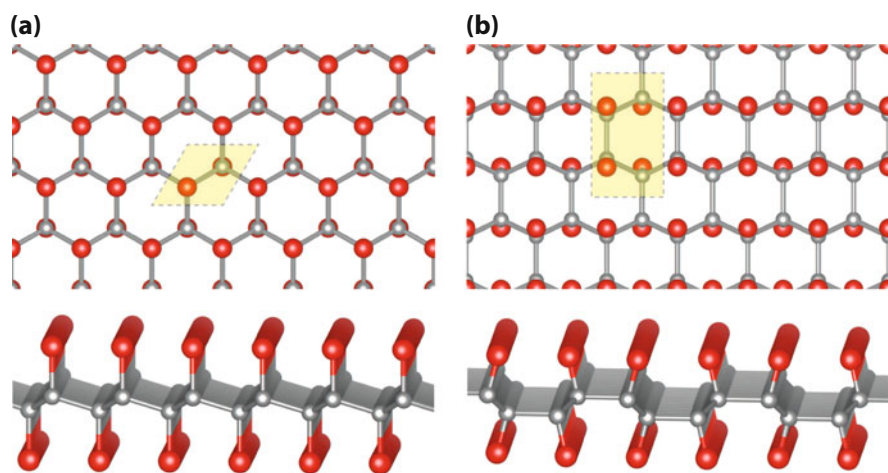


Fig. 2.8 Atomic structures of (a) chair and (b) boat conformers of fully hydrogenated silicene. Primitive unitcells of the structures are highlighted by *yellow color*

electronic properties of hydrogenated silicene (and germanene counterparts) using the ab-initio DFT methodology (Lew Yan Voon et al. 2010). It was reported that the buckling of silicene increases from 0.44 to 0.72 Å upon full hydrogenation. Their structural analysis on silicene and germanane revealed that the chair configuration is energetically favored over the boat structure. Voon et al. also reported that full hydrogenation opens a large bandgap in the silicene's electronic structure,

typically, in the 3–4 eV range for silicane (with LDA, the approximated value is only 2 eV). In their analysis, where the spin-orbit interaction was ignored, it was shown that semimetallic silicene (germanene) turns into an indirect (a direct) bandgap semiconductor. Tight-binding parameters for silicane and germanane were also derived (Zólyomi et al. 2014).

Similarly, Houssa et al. performed first principles calculations based on DFT, within LDA, HSE and GW, to investigate the electronic properties of silicane and germanane. They predicted that two different configurations (chairlike and boatlike) are equally stable, and, depending on the synthesis procedure, that both configurations can be formed. While the chair configuration of silicane is an indirect semiconductor, the boat structure is found to be a direct bandgap material in all approaches (LDA, HSE and GW). It was also shown that chairlike germanane is a direct gap semiconductor with an energy bandgap of 3.5 eV, which makes it useful for optical applications in the blue/violet range (Houssa et al. 2011).

Following these preliminary studies many groups have shown that silicane forms a chairlike structure in its ground state. Although, the presence of an indirect electronic bandgap is one of the main disadvantage of silicane, its employ in opto-electronic device applications still can be realized by making use of hydrogenated bilayer silicene. As shown by Huang et al., in contrast with single layer silicene and silicane, hydrogenated bilayer silicene is optically active and a promising material for the optical applications (Huang et al. 2014). It was also concluded that depending on hydrogen concentrations double-sided SiH_x structures can have direct (or quasidirect) band gaps within the range of RGB colors, which shows that these double-sided SiH_x structures can be used as light emitters for white LEDs (Fig. 2.9).

The substrate plays an important role in determining the structural and electronic properties of silicene-based materials (see Chap. 3). In a theoretical study which takes into account the effect of the substrate it was shown that the coverage and arrangement of the absorbed hydrogen atoms on silicene changed significantly the electronic properties, such as the direct/indirect band gaps or metallic/semiconducting features (Zhang et al. 2012). They also reported that half-hydrogenated silicene with chair-like structure had ferromagnetic character.

One of the main drawback of silicene and silicane studies is that synthesis of their free standing monolayer crystals have not been achieved so far. However, Qiu et al. demonstrated the possibility of ordered and reversible hydrogenation of silicene on an Ag(111) substrate. In their study, by combining *ab initio* DFT calculations and scanning tunneling microscopy measurements (Qiu et al. 2015), it was found that hydrogenation of silicene at room temperature results in formation of perfectly ordered γ -(3×3) superstructure. Moreover, when the reconstructed hydrogenated silicene sheet is heated up to 450 K, dehydrogenation takes place and the surface restores to its initial form which is pristine silicene layer. Such a reversible reaction of silicene sheets with hydrogen allows tunable crossover between semiconducting and metallic phases.

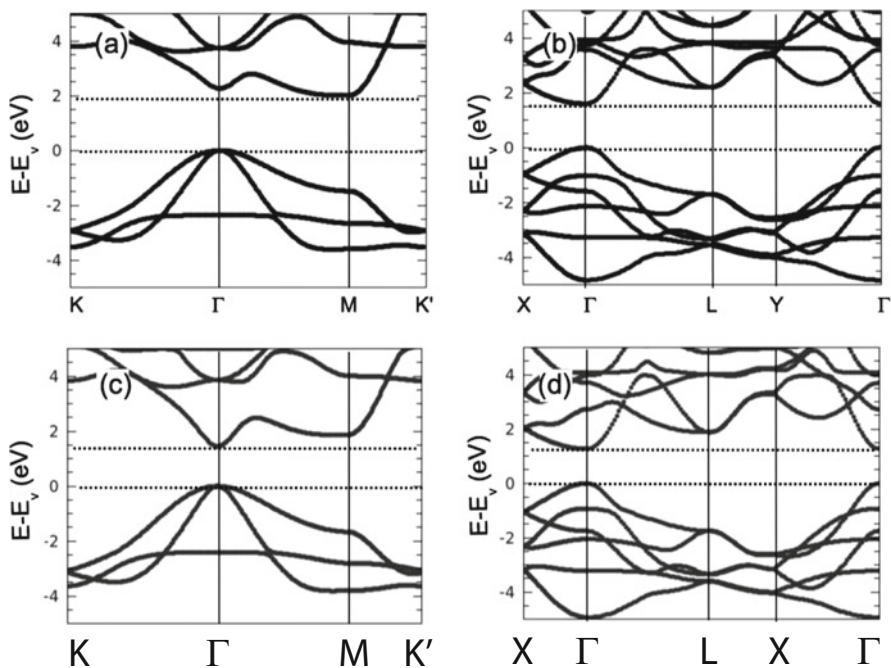


Fig. 2.9 Energy band structures, calculated using the LDA functional, for (a) chairlike silicene, (b) boatlike silicene, (c) chairlike germanane, and (d) boatlike germanane. The reference zero energy level corresponds to the top of the valence band. Adapted from Houssa et al. (2011)

The in-plane thermal conductivity of graphene, as a consequence of quantum confinement in 2D, is the highest among well-known materials. Therefore, one can expect high thermal transport and specific heat also in silicene and related materials. Classical molecular dynamics calculations of graphene supported silicene revealed that the thermal transport behavior of such hetero-interfaces can be dramatically tuned by hydrogenation (Liu et al. 2014). It was found that by changing the hydrogen coverage the thermal conductivity can be controllably manipulated and maximized up to five times larger than that of pristine silicene/graphene hetero-interface.

Ferromagnetism in monolayer crystal structures is essential for nanoscale spintronics device applications. Hydrogenation is also an efficient way of inducing ferromagnetism in silicene. It was demonstrated that half-hydrogenation breaks the extended π -bonding network of silicene, leaving the electrons in the unsaturated Si atoms localized and unpaired, and thus it exhibits ferromagnetic semiconducting behavior with a band gap of 0.95 eV. The long-range ferromagnetic coupling between Si atoms was also predicted by Zhang and Yan, with a Curie temperature of about 300 K (Zhang and Yan 2012).

Full hydrogenation of germanene, the first synthesis of germanane, was successfully achieved by Bianco et al. in 2013. The hydrogenated germanene (with the chemical formula GeH) is obtained from the topochemical deintercalation of CaGe₂ (Bianco et al. 2013). The obtained GeH monolayers GeHs are thermally stable up to 75 °C, but above this temperature amorphization and dehydrogenation begin to occur. These authors also demonstrated that easy transfer of these single crystals can be achieved through mechanical exfoliation onto SiO₂/Si surfaces. The theoretically predicted bandgap of 1.53 eV and the high electron mobility which is five times higher than for bare germanene of germanane show the potential use in optoelectronic device applications.

2.5 Oxygenation

Due to its technological importance, the interaction of graphitic materials with oxygen has always been one of the main focus of materials science. It has been reported by many groups that synthesis of new products can be achieved by either a chemical reaction or by gaseous diffusion of oxygen through the material. However, in contrast to single crystals of halogenated graphenes, formation of a well-ordered oxidized monolayer graphene has never been achieved so far. Instead, researchers synthesized grapheneoxides (GOs) which is composed of a graphene layer surrounded by many hydrocarbons and chemical impurities.

It was demonstrated that oxidation leads to dramatic changes in the structural and electronic properties of silicene. While the binding energy of silicene on Ag surface is around 0.7 eV, Si-O bonds have binding energy of 4–12 eV (Xu et al. 2014; Zhang et al. 2001). As shown in Fig. 2.10, oxygen adatoms prefer to form Si-O-Si bonds at bridge sites in the 3×3 silicene surface without resulting in any deformation on the Ag substrate. ARPES measurements revealed that oxidation of silicene breaks the Si-Ag hybridization and that the Ag(111) Shockley surface state can be revived. It was also reported that after the oxidation process, the semimetallic behavior disappears and the silicene oxide exhibits a disordered structure with a semiconductor-like character. Similarly, by performing low-temperature scanning tunneling microscopy and in situ Raman spectroscopy measurements it was shown that depending on the adsorption configurations and amounts of oxygen adatoms on the silicene surface different buckled structures with different bandgaps can be obtained (Du et al. 2014). In addition, very recently the microscopic mechanism of the reaction of O₂ with silicene was studied by first-principles molecular dynamics simulations. It was found that oxidation of the surface is accelerated by the synergetic effect of molecular O₂ dissociation and subsequent local structural relaxations (Morishita and Spencer 2015).

Partial and full oxidation of silicene has been studied in detail (Wang et al. 2013; Özçelik et al. 2014). Depending on the amount and type of oxidizing agents, the honeycomb structure of silicene may be preserved, distorted or destroyed.

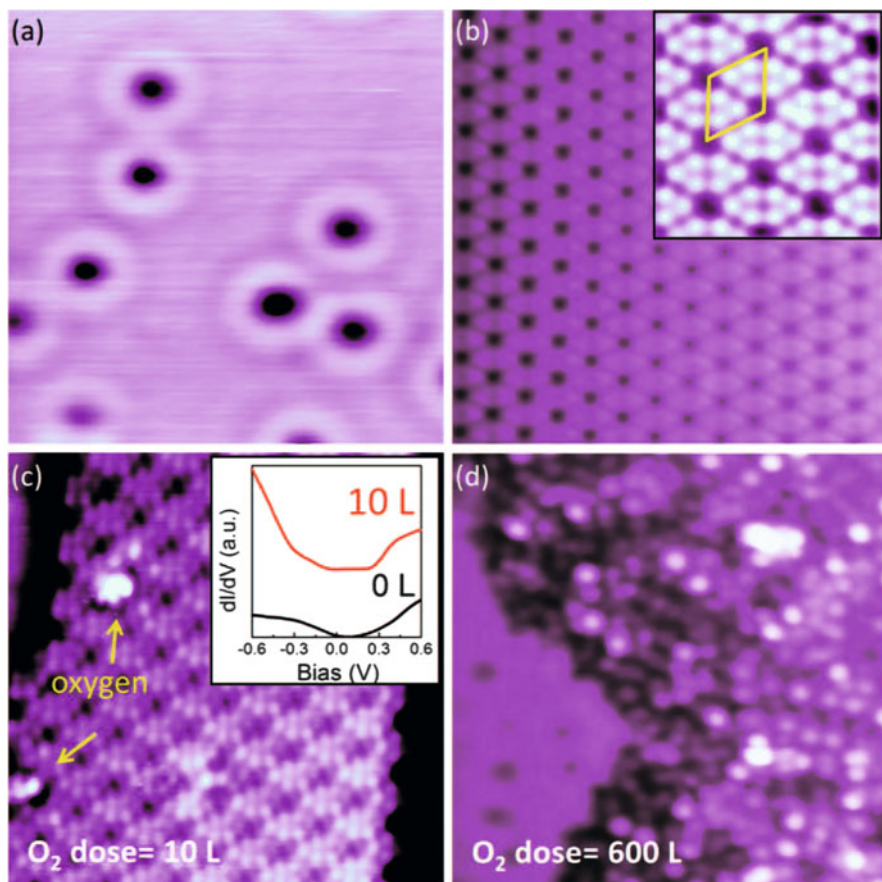


Fig. 2.10 (a) STM topographical image of clean Ag(111) substrate, (b) 3×3 silicene on 4×4 Ag(111), (c) STM image of silicene layer oxidized by an oxygen dose of 10 L. O adatoms prefer to reside at bridge sites. The inset contains STS spectra of silicene and silicene oxide samples, indicating that there is gap opening due to oxidation. (d) STM image of the 3×3 silicene sheet oxidized under 600 L O_2 . The bare Ag(111) surface can be seen at the *bottom left* of (d). Adapted from Xu et al. (2014)

The properties of the resulting materials also vary significantly from metals and semimetals to semiconductors and insulators (Wang et al. 2013). The 2D honeycomb counterpart of α -quartz was also shown to be stable (Özçelik et al. 2014). The geometry of this structure is composed of reentrant Si-O bonds which makes its Poisson ratio negative. When pulled in a certain direction, such auxetic materials enlarge (instead of shrinking) in the perpendicular direction. 2D α -quartz also has a high piezoelectric coefficient and its nanoribbons show metallic or semiconducting behavior depending on their chirality (Özçelik et al. 2014).

2.6 Interaction with Halogens

Halogenation is the general term used for reaction of an alkene structure with a halogen atom. When an alkene interacts with a halogen atom, reaction takes place at the carbon-carbon double bond. Regarding monolayer crystal structures, the first example of full halogenation was achieved using XeF_2 leading to a fully fluorinated structure, which is called fluorographene, is a high-quality insulator (resistivity $> 10^{12} \Omega$) with an optical gap of 3 eV (Nair et al. 2010). It inherits the mechanical strength of graphene, exhibiting a Young's modulus of 100 N m^{-1} and sustaining strains of 15 %. Fluorographene is inert and stable up to 400°C even in air, similar to Teflon. Moreover, even if bare graphene does not interact with molecular Chlorine, experimental realization of chlorination of graphene can be achieved by using a photochlorination technique (Li et al. 2011).

Since silicene electronically and structurally shares some of the unique properties of graphene, one may expect similar properties upon halogenation of silicene. Recently, the geometry, electronic structure and mechanical properties of halogenated silicene SiX ($\text{X} = \text{F}, \text{Cl}, \text{Br}$ and I) in various conformers were studied using first-principles calculations within the DFT (Zhang et al. 2015). Chair conformation of fluorinated and chlorinated silicenes are alike those in Fig. 2.8a. It was shown that halogenated silicene has enhanced stability compared to silicene, a moderate and tunable direct gap, and small carrier masses. The element- and conformer-dependence of the energy gap could be well understood by the variance of buckling and a bond energy perturbation theory based on orbital hybridization (Fig. 2.11).

Many-body effects in fluorosilicene and silicane, as well as armchair silicene nanoribbons (ASiNRs) were studied using Green's function perturbation theory (Wei and Jacob 2013). It was found that in addition to the remarkable self-energy

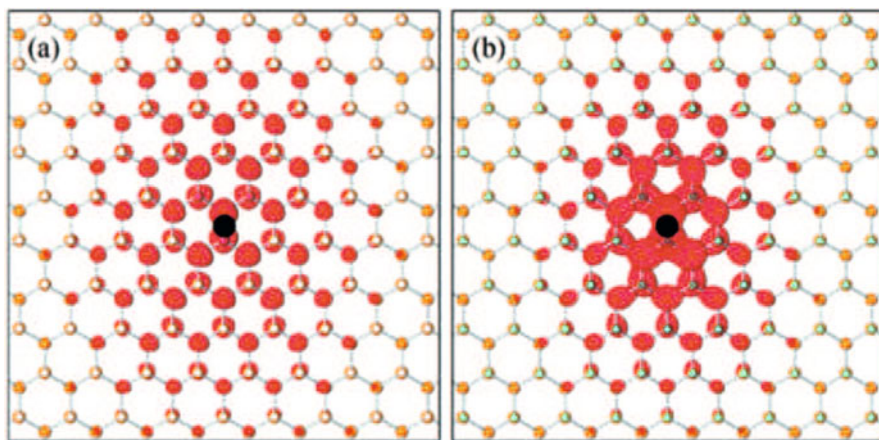


Fig. 2.11 Electron probability distribution for the first bound excitonic state of (a) silicane and (b) fluorosilicene. Adapted from Wei and Jacob (2013)

effects, the optical absorption properties of silicane and fluorosilicene are dominated by strong excitonic effects with formation of bound excitons with considerable binding energies.

Moreover, the structural, electronic and magnetic properties of half-fluorinated silicene sheets were investigated using first-principles simulation in the framework of DFT (Wang et al. 2015). They reported that half-fluorinated silicene sheets with zigzag, boat-like or chair-like configurations were confirmed as dynamically stable based on phonon calculations. Upon the adsorption of fluorine, direct energy band gaps opened in both zigzag and boat-like conformations. Moreover, the half-fluorinated silicene with chair-like configuration showed an antiferromagnetic behavior that mainly stems from fluorine-free Si atoms.

Recently, two-dimensional 2D topological insulators (TIs) in functionalized germanenes (GeX, X = H, F, Cl, Br, or I) were proposed (Si et al. 2014). It was found that GeI is a 2D TI with a bulk gap of about 0.3 eV, while GeH, GeF, GeCl, and GeBr can be transformed into TIs with sizable gaps under achievable tensile strains. They reported that the coupling of the p_{xy} orbitals of Ge and heavy halogens in forming the σ orbitals also plays a key role in the further enlargement of the gaps in halogenated germanenes.

2.7 Functionalization of Silicene

Functionalization of silicene by various adatoms has been studied extensively (Sahin and Peeters 2013; Sivek et al. 2013; Özçelik and Ciraci 2013). The interaction of silicene with metal adatoms is quite strong compared to graphene (Sahin and Peeters 2013). Alkali metals like Li, Na, and K, adsorb to the hollow sites without distorting the lattice. Upon significant charge transfer, silicene becomes metallic. Adsorption of alkaline-earth metals like Be, Mg and Ca, on the other hand, turns silicene into a narrow gap semiconductor. Silicene becomes half-metallic when it is functionalized by transition metal adatoms like Ti and Cr (Sahin and Peeters 2013).

Adsorption of Al and P, that are group III and V elements from the Si row, result in dumbbell structures discussed below (Sivek et al. 2013). Adsorption of B also makes a dumbbell structure, while a N adatom prefers the bridge site of silicene. Both adsorption and substitution of these group III and V elements make silicene metallic. As shown in Fig. 2.12, adsorption/substitution of first-row elements do not result in a significant change in the phonon DOS. Due to the coupling of B and N adsorbates/substituents to the acoustical phonon branch of pristine silicene, several sharp peaks appear between 200 and 300 cm^{-1} . Obviously, among the two adsorbates nitrogen atoms are more likely to mix with silicene's acoustic phonons. In addition to these, high-frequency adsorbate/substituent induced modes appear between 700 and 1200 cm^{-1} . As shown in the Fig. 2.12, these high energy modes correspond to in-plane bond-stretching motion of the adatom and the neighboring silicon atoms. However, since the second row elements Al and P have similar atomic weights with Si, their adsorption/substitution modifies the vibrational spectra

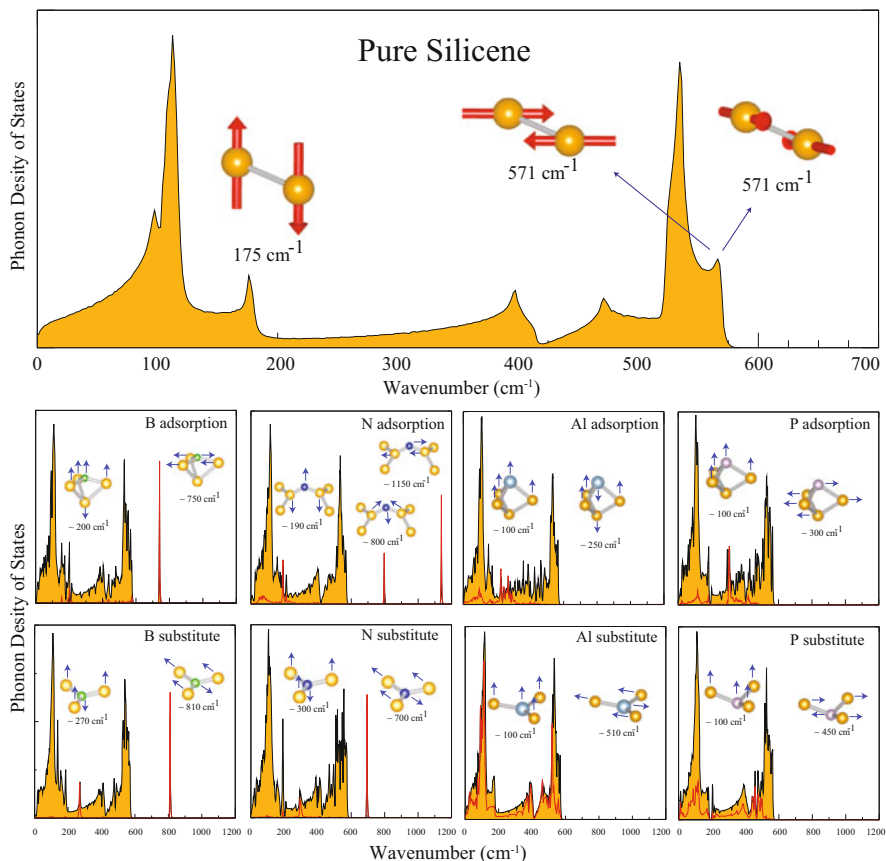


Fig. 2.12 Phonon density of states for adsorption and substitution cases of B, N, Al and P on silicene. The total DOS of the structures are shown by the *filled area*. The projected DOS belonging to foreign atoms are represented by *red lines*. Gamma point vibrational motions are also depicted

of silicene in a different way. As seen from Fig. 2.12, the characteristic behavior of second row elements is the absence of high-frequency bond stretching modes. It is also seen that while substituent B and N atoms do not couple with optical modes of silicene, Al and P atoms entirely contribute to both acoustic and optical modes. While the presence of first row elements B and N can be monitored by Raman spectroscopy measurements, second-row elements Al and P have no clear fingerprint in their phonon dispersion.

The presence of Stone-Wales defects, i.e. a pentagon associated to a heptagon, can significantly affect the site preference of adatoms (Sahin et al. 2013). A N adatom, for example, prefers to attach to defect-free sites. The energy barrier for the formation of Stone-Wales defects in freestanding silicene was shown to be much smaller compared to that of graphene (Sahin et al. 2013; Özçelik et al. 2013).

2.8 Dumbbell Structure

One of the most interesting cases occur when the adatom is also silicon. A Si adatom first attaches to dangling bonds of silicene and then forms bridge bonds with two-second neighbor Si atoms of silicene thereby increasing the coordination number of these Si atoms from three to four. In search for tetrahedral orientation, these four bonds then force the atoms to move towards the directions shown in the middle panel of Fig. 2.13. As a result, the new Si adatom sits 1.38 Å above the top site of silicene while at the same time pushing down the Si atom just below it by the same amount. These two atoms are connected to other Si atoms by three bonds that are almost perpendicular to each other. The resulting geometry is called the dumbbell (DB) structure (Özçelik and Ciraci 2013; Kaltsas and Tsetseris 2013; Cahangirov et al. 2014). The DB formation is an exothermic process and occurs spontaneously without need to overcome any kind of barrier. In the case of a C adatom adsorbed on graphene, the DB structure does not form because it is energetically less favorable compared to the configuration in which the C adatom is attached to the bridge site of graphene (Özçelik et al. 2013).

Calculations show that when a single DB unit is placed in an $n \times n$ unit cell the cohesive energy per Si atom is maximized when $n = \sqrt{3}$ and decreases monotonically for $n \geq 2$ (Cahangirov et al. 2014). We refer to the structure having a single DB unit in the $\sqrt{3} \times \sqrt{3}$ unit cell as trigonal dumbbell silicene (TDS) due to the trigonal lattice formed by DB atoms, as shown in Fig. 2.14a (Kaltsas and Tsetseris 2013; Cahangirov et al. 2014). As seen in Table 2.1, TDS is energetically more favorable than freestanding silicene (Özçelik and Ciraci 2013; Kaltsas and Tsetseris 2013). Interestingly, the cohesive energy per Si atom is further increased when another DB unit is created in the $\sqrt{3} \times \sqrt{3}$ unit cell of TDS. We refer to this new structure as honeycomb dumbbell silicene (HDS) due to the honeycomb structure formed by two DB units in the $\sqrt{3} \times \sqrt{3}$ unit cell (see Fig. 2.14b). The

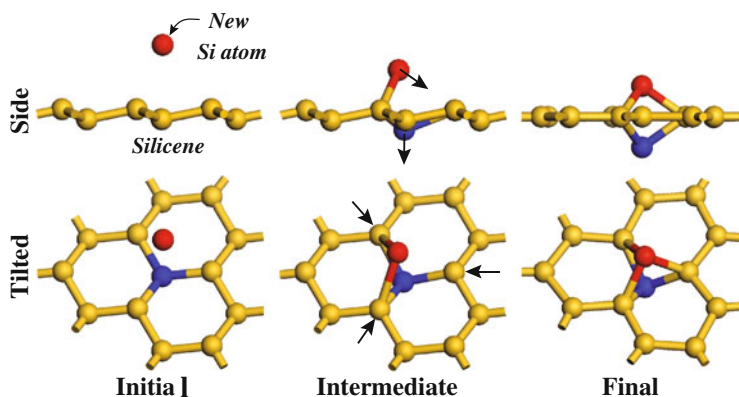


Fig. 2.13 Formation of the dumbbell building block units starting from freestanding silicene

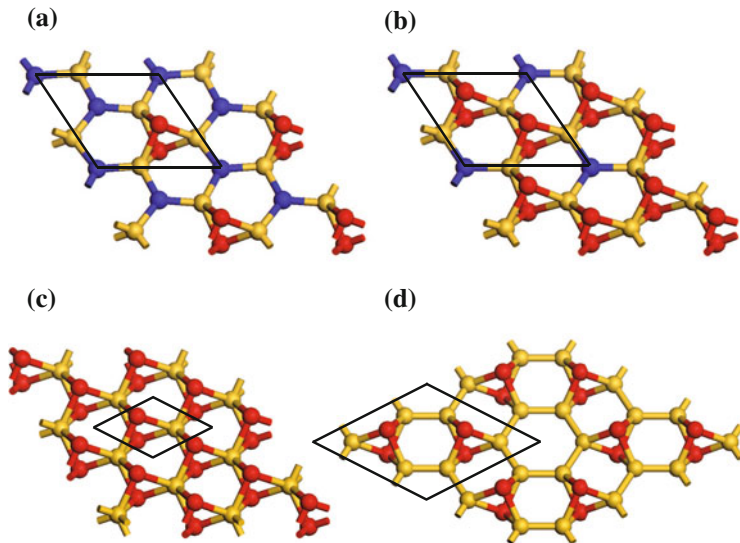


Fig. 2.14 Atomic structure of (a) $\sqrt{3} \times \sqrt{3}$ trigonal dumbbell silicene (TDS), (b) $\sqrt{3} \times \sqrt{3}$ honeycomb dumbbell silicene (HDS), (c) 1×1 full dumbbell silicene (FDS) and (d) 2×2 large honeycomb dumbbell silicene (LHDS). The unit cells are delineated by solid black lines. Atoms having different environment are represented by balls having different colors

Table 2.1 Cohesive energy and $\sqrt{3} \times \sqrt{3}$ lattice constant of slightly buckled silicene compared with that of dumbbell structures

	Silicene	TDS	LHDS	HDS	FDS
Cohesive energy (eV/atom)	3.958	4.013	4.161	4.018	3.973
$\sqrt{3} \times \sqrt{3}$ lattice constant (Å)	6.69	6.52	6.43	6.38	6.23

atomic structure of HDS is crucial to understand the $\sqrt{3} \times \sqrt{3}$ reconstruction that emerges when silicene is epitaxially grown on Ag(111) substrates (Cahangirov et al. 2014; Feng et al. 2012; Chen et al. 2012; Vogt et al. 2014). Adding another DB unit in the $\sqrt{3} \times \sqrt{3}$ unit cell of HDS results in a 1×1 structure composed of DB atoms connected by sixfold coordinated Si atoms (see Fig. 2.14c). The cohesive energy of this structure, that we refer to as full dumbbell silicene (FDS), is less than that of TDS and HDS.

We should emphasize that it is the interplay between two competing effects that makes HDS the most favorable $\sqrt{3} \times \sqrt{3}$ structure. While formation of new DBs and thus new bonds increases the cohesive energy, the increase in the coordination number beyond four decreases it. As seen in Fig. 2.14, the coordination number of yellow atoms in the TDS structure is four while in HDS it is five. Apparently, the formation of a new DB and hence new bonds compensates the energy required to form the peculiar five-fold coordination. However, it fails to compensate the six-fold coordination of Si atoms forming the middle atomic layer of FDS. This arguments led us to investigate another DB structure that has even larger cohesive energy per

atom compared to HDS. This structure has two DB units arranged in a honeycomb lattice in a 2×2 unit cell. Here the packing of DB units is dense compared to TDS but sparse compared to HDS. In this structure, the honeycomb lattice formed by dumbbell units is larger compared to the one formed in HDS, hence we refer to this structure as large honeycomb dumbbell silicene (LHDS). As seen in Fig. 2.14d, the maximum coordination of Si atoms in the LHDS is four. Since there are more DB units in LHDS compared to TDS and no hypervalent Si atoms as in HDS, the cohesive energy per atom of freestanding LHDS is higher than both TDS and HDS.

In Fig. 2.15a we show the calculated phonon dispersions of the TDS, LHDS, HDS and FDS structures, showing that the frequencies of all the modes are positive

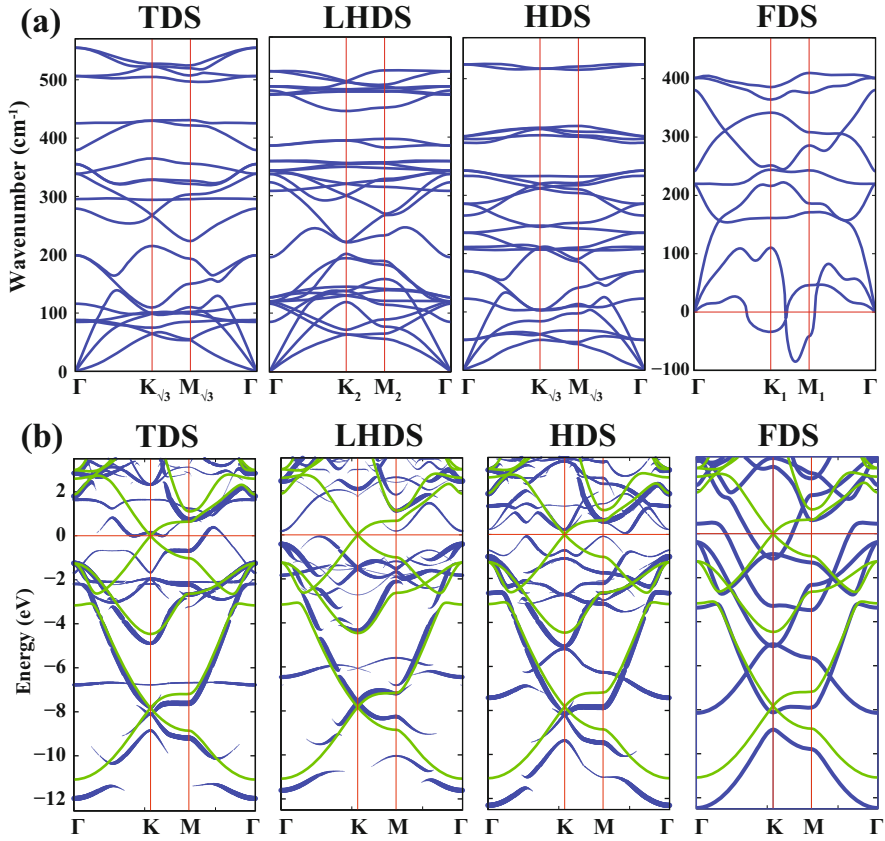


Fig. 2.15 (a) The phononic band dispersions of the TDS, LHDS, HDS and FDS structures. The K and M points in the BZs of the 1×1 , 2×2 and $\sqrt{3} \times \sqrt{3}$ unit cells are indicated by subscripts. (b) The electronic band dispersions of the TDS, LHDS and HDS structures unfolded to the BZ of the free-standing 1×1 silicene. The thickness of the *blue line* at a certain point of the Brillouin zone is proportional to the weight of that state in the unfolded band (Allen et al. 2013). The bands of the FDS structure do not need to be unfolded because it has 1×1 periodicity. The superimposed electronic band structures of the free-standing 1×1 silicene are shown by *green lines*

over the whole Brillouin zone (BZ) in the TDS, LHDS and HDS, cases while there are imaginary frequencies near the BZ boundary in the FDS one. This means that TDS, LHDS and HDS are thermodynamically stable structures while FDS is unstable. This also implies that the stability of TDS, LHDS and HDS structures does not depend on the substrate and thus these structures can exist in their freestanding configuration.

In Fig. 2.15b we present the electronic band dispersions of DB silicene structures. To compare with free-standing silicene we unfold the bands of all structures into the BZ of the 1×1 primitive cell, except that of FDS, which already has this periodicity (Cahangirov et al. 2014). The structures are intentionally ranked starting with TDS in which DB units are the most sparse and ending with FDS in which they are the densest. In this way, one can immediately see how the flat band around -7 eV that comes from the weakly-interacting DB units of TDS is gradually turned into the highly-dispersive (~ 1.5 eV) band that comes from the strong interaction between DB units that are densely packed in the FDS structure. While this deep band of FDS is easily traced back to TDS the other band of FDS that is originating from the DB units appears much higher and crosses the Fermi level. It is much harder to clearly associate this latter band with its counterparts in TDS, LHDS or HDS. This indicates that in these structures there is a complex interaction between the states originating from the DB units and the π -states coming from other Si atoms. These results might be used in experiments to identify the formation of DB units.

2.9 Nanoribbons

The atomic and electronic structures of zigzag and armchair silicene nanoribbons was studied in detail (Cahangirov et al. 2009, 2010). As seen in Fig. 2.16, both zigzag and armchair silicene nanoribbons (SiNR) acquire a 2×1 reconstruction when the edges are not saturated. In Fig. 2.16c we compare the total energies of two nonmagnetic and two magnetic structures. The difference between the two nonmagnetic structures is the position of one of the edge atoms denoted by 1 and 2. In the geometry denoted by 1, the corresponding edge atom significantly deviates from the nanoribbon plane thereby gaining enough energy to make this nonmagnetic structure the ground state. This metallic nonmagnetic ground state is in contrast to semiconducting zigzag graphene nanoribbons that have localized states along their edges with opposite spins. One can take advantage of this property to make zigzag graphene nanoribbons half-metallic by applying an in-plane homogeneous electric field (Son et al. 2006b). It was shown that, zigzag SiNRs can acquire magnetic properties through hydrogen saturation at the edges (Zborecki et al. 2014b). Furthermore, when doped with N atoms, zigzag SiNRs become half-metallic with opposite spins making up the conduction and valence band edge states that touch each other at the Fermi level (Zheng et al. 2013).

Both bare and hydrogen saturated armchair nanoribbons of silicene and germanene are semiconductors and show family behavior in their band gaps with

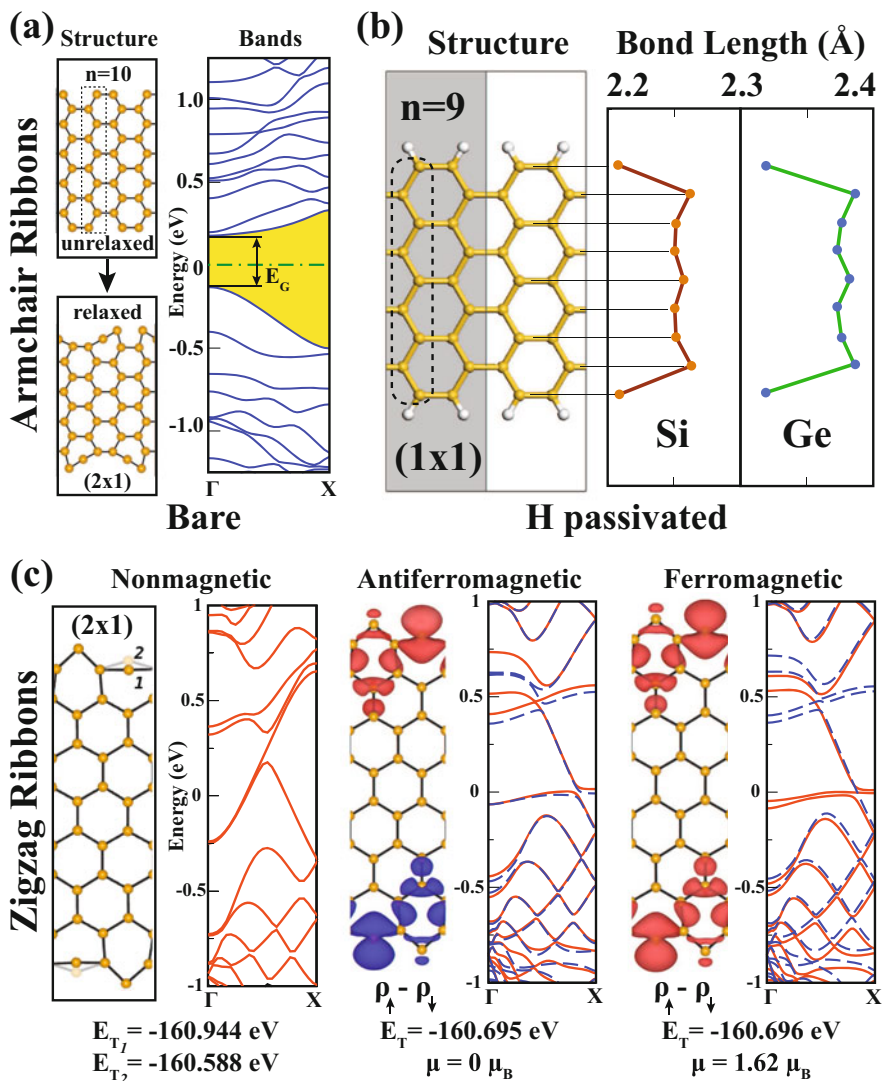


Fig. 2.16 (a) Atomic structure of bare armchair silicene nanoribbon (SiNR) with $n=10$ atoms (which defines the width) in a 1×1 unitcell. Upon relaxation edge atoms get reconstructed and the unitcell is doubled. Band structure of optimized bare armchair SiNR with $n=10$ width. (b) Atomic structure and bond length alternation of hydrogen passivated armchair SiNR with width $n=9$. (c) Atomic and electronic structure of nonmagnetic and magnetic states of 2×1 reconstructed zigzag silicene nanoribbons. The isosurface of the total charge density difference between the up-spin and the down-spin states are given for the antiferromagnetic and ferromagnetic states (Cahangirov et al. 2009, 2010)

respect to their widths (Cahangirov et al. 2010). It means that, if one chooses three armchair nanoribbons having $3k-1$, $3k$ and $3k+1$ atoms per unit cell, where k is a positive integer, then the former will have the lowest gap, the latter will have the largest gap while the middle one will have a gap that is in between. As k is increased, the band gaps of all three families approach to zero, due to the quantum confinement (and the fact that 2D silicene is a semimetal) as illustrated in Fig. 2.17a. This trend originates from the folding of the band structure of silicene and germanene and the same is also true for the armchair graphene nanoribbons (Son et al. 2006a). This property was experimentally confirmed in the case of graphene nanoribbons using lithographic processes (Han et al. 2007).

The family behavior in armchair SiNRs can be reproduced using a much simpler two-parameter tight-binding model that also works in the case of armchair graphene nanoribbons (Son et al. 2006a). Here one starts by noting that the bond length is almost constant throughout the hydrogen passivated armchair nanoribbons of silicene and germanene, except for the sudden decrease at the edges, as illustrated in Fig. 2.16b. Hence, two hopping parameters are defined; one for the edges and

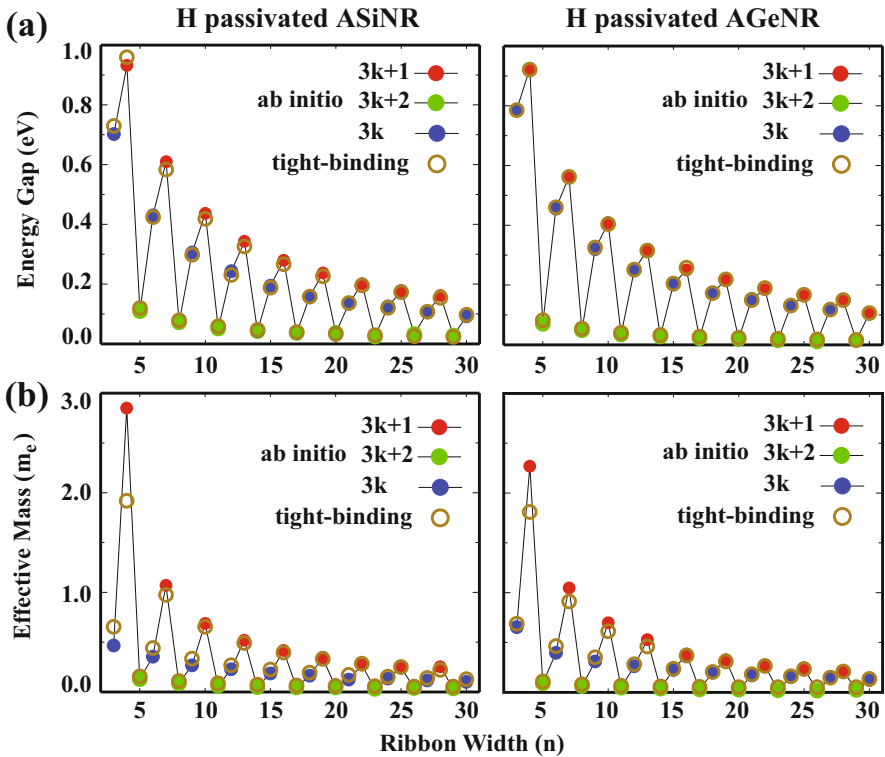


Fig. 2.17 The family behavior in (a) the energy gaps and (b) effective masses of hydrogen saturated nanoribbons of silicene and germanene. Adapted from Cahangirov et al. (2010)

another for the rest of the structure. Since the bond lengths are smaller at the edges, the corresponding hopping is slightly higher. As seen in Fig. 2.17, it is possible to reproduce both energy gaps and the effective masses of the first conduction bands by manually fitting these two parameters. As a result of this fitting, the tight-binding parameters were determined for hydrogen saturated silicene and germanene armchair nanoribbons to be $t_{Si} = 1.03$ eV, $t_{Ge} = 1.05$ eV, $t_{Si,edge} = 1.15$ eV, and $t_{Ge,edge} = 1.13$ eV. Interestingly, the ratio of the two tight binding parameters is the same for graphene and silicene.

The confinement of electrons was studied in superlattices formed by armchair SiNRs having different widths (Cahangirov et al. 2010). Here computationally feasible structures were calculated using ab-initio techniques and it was verified that the aforementioned tight-binding model works even for such unusual geometries. Then, much larger systems were investigated by the tight-binding model. It was possible to explain the obtained confinement trends using the family behavior and also including the effects due to the interface.

The thermoelectric properties of silicene and of its nanoribbons were also studied in detail (Hu et al. 2013; Zborecki et al. 2013, 2014a; Yang et al. 2014; An et al. 2014; Wierzbicki et al. 2015). The thermal conduction of silicene and SiNRs significantly increases with applied tensile strain until reaching a plateau, in contrast to graphene which has lower thermal conductivity when stretched (Hu et al. 2013). This was explained by the fact that the out-of-plane flexural phonon modes of silicene are stiffened with applied tensile strain while in the case of graphene they are softened. The in-plane transverse and longitudinal modes, on the other hand, are softened in both silicene and graphene which also explains the plateau observed in silicene at high strain. Doping zigzag SiNRs with Al and P atoms increases the Seebeck coefficient (Zborecki et al. 2014a). The figures of merit of thermoelectric energy conversion were found to be approaching and in some cases passing 1 for the narrow SiNRs (Yang et al. 2014). Finally, single spin negative differential resistance and strong spin Seebeck effect can be achieved by engineering defects on zigzag SiNRs (An et al. 2014).

References

- Abersfelder, K., White, A.J.P., Rzepa, H.S., Scheschkewitz, D.: A tricyclic aromatic isomer of hexasilabenzene. *Science* **327**, 564–566 (2010)
- Allen, P.B., Berlijn, T., Casavant, D.A., Soler, J.M.: Recovering hidden Bloch character: unfolding electrons, phonons, and slabs. *Phys. Rev. B* **87**, 085322 (2013)
- An, R.L., Wang, X.F., Vasilopoulos, P., Liu, Y.S., Chen, A.B., Dong, Y.J., Zhai, M.X.: Vacancy effects on electric and thermoelectric properties of zigzag silicene nanoribbons. *J. Phys. Chem. C* **118**, 21339–21346 (2014)
- Barton, T.J., Burns, G.T.: Unambiguous generation and trapping of a silabenzene. *J. Am. Chem. Soc.* **100**, 5246–5246 (1978)
- Bianco, E., Butler, S., Jiang, S., Restrepo, O.D., Windl, W., Goldberger, J.E.: Stability and exfoliation of germanane: a germanium graphene analogue. *ACS Nano* **7**, 4414–4421 (2013)
- Blöchl, P.E.: Projector augmented-wave method. *Phys. Rev. B* **50**, 17953–17979 (1994)

- Brumfiel, G.: Sticky problem snares wonder material. *Nature* **495**, 152–153 (2013)
- Cahangirov, S., Topsakal, M., Aktürk, E., Şahin, H., Ciraci, S.: Two- and one-dimensional honeycomb structures of silicon and germanium. *Phys. Rev. Lett.* **102**, 236804 (2009)
- Cahangirov, S., Topsakal, M., Ciraci, S.: Armchair nanoribbons of silicon and germanium honeycomb structures. *Phys. Rev. B* **81**, 195120 (2010)
- Cahangirov, S., Özçelik, V.O., Xian, L., Avila, J., Cho, S., Asensio, M.C., Ciraci, S., Rubio, A.: Atomic structure of the $\sqrt{3} \times \sqrt{3}$ phase of silicene on Ag(111). *Phys. Rev. B* **90**, 035448 (2014)
- Chen, L., Liu, C.C., Feng, B., He, X., Cheng, P., Ding, Z., Meng, S., Yao, Y., Wu, K.: Evidence for Dirac fermions in a honeycomb lattice based on silicon. *Phys. Rev. Lett.* **109**, 056804 (2012)
- Cudazzo, P., Attaccalite, C., Tokatly, I.V., Rubio, A.: Strong charge-transfer excitonic effects and the Bose-Einstein exciton condensate in graphane. *Phys. Rev. Lett.* **104**, 226804 (2010)
- Drummond, N.D., Zólyomi, V., Fal'ko, V.I.: Electrically tunable band gap in silicene. *Phys. Rev. B* **85**, 075423 (2012)
- Du, Y., Zhuang, J., Liu, H., Xu, X., Eilers, S., Wu, K., Cheng, P., Zhao, J., Pi, X., See, K.W., Peleckis, G., Wang, X., Dou, S.X.: Tuning the band gap in silicene by oxidation. *ACS Nano* **8**, 10019–10025 (2014)
- Elias, D.C., Nair, R.R., Mohiuddin, T.M.G., Morozov, S.V., Blake, P., Halsall, M.P., Ferrari, A.C., Boukhalov, D.W., Katsnelson, M.I., Geim, A.K., Novoselov, K.S.: Control of graphene's properties by reversible hydrogenation: evidence for graphane. *Science* **323**, 610–613 (2009)
- Ezawa, M.: Valley-polarized metals and quantum anomalous Hall effect in silicene. *Phys. Rev. Lett.* **109**, 055502 (2012)
- Feng, B., Ding, Z., Meng, S., Yao, Y., He, X., Cheng, P., Chen, L., Wu, K.: Evidence of silicene in honeycomb structures of silicon on Ag(111). *Nano Lett.* **12**, 3507–3511 (2012)
- Guzmán-Verri, G.G., Lew Yan Voon, L.C.: Electronic structure of silicon-based nanostructures. *Phys. Rev. B* **76**, 075131 (2007)
- Han, M.Y., Özyilmaz, B., Zhang, Y., Kim, P.: Energy band-gap engineering of graphene nanoribbons. *Phys. Rev. Lett.* **98**, 206805 (2007)
- Hoffmann, R.: Small but strong lessons from chemistry for nanoscience. *Angew. Chem. Int. Ed.* **52**, 93–103 (2013)
- Houssa, M., Scalise, E., Sankaran, K., Pourtois, G., Afanas'ev, V.V., Stesmans, A.: Electronic properties of hydrogenated silicene and germanene. *Appl. Phys. Lett.* **98**, 223107 (2011)
- Hu, M., Zhang, X., Poulikakos, D.: Anomalous thermal response of silicene to uniaxial stretching. *Phys. Rev. B* **87**, 195417 (2013)
- Huang, B., Deng, H.X., Lee, H., Yoon, M., Sumpter, B.G., Liu, F., Smith, S.C., Wei, S.H.: Exceptional optoelectronic properties of hydrogenated bilayer silicene. *Phys. Rev. X* **4**, 021029 (2014)
- Jahn, H.A., Teller, E.: Stability of polyatomic molecules in degenerate electronic states. I. orbital degeneracy. *Proc. R. Soc. Lond. A Math. Phys. Eng. Sci.* **161**, 220–235 (1937)
- Kaltsas, D., Tsetseris, L.: Stability and electronic properties of ultrathin films of silicon and germanium. *Phys. Chem. Chem. Phys.* **15**, 9710–9715 (2013)
- Kresse, G., Joubert, D.: From ultrasoft pseudopotentials to the projector augmented-wave method. *Phys. Rev. B* **59**, 1758–1775 (1999)
- Krüger, P., Pollmann, J.: Dimer reconstruction of diamond, Si, and Ge (001) surfaces. *Phys. Rev. Lett.* **74**, 1155–1158 (1995)
- Lander, J.J., Gobeli, G.W., Morrison, J.: Structural properties of cleaved silicon and germanium surfaces. *J. Appl. Phys.* **34** (1963)
- Lew Yan Voon, L.C., Sandberg, E., Aga, R.S., Farajian, A.A.: Hydrogen compounds of group-iv nanosheets. *Appl. Phys. Lett.* **97**, 163114 (2010)
- Li, B., Zhou, L., Wu, D., Peng, H., Yan, K., Zhou, Y., Liu, Z.: Photochemical chlorination of graphene. *ACS Nano* **5**, 5957–5961 (2011)
- Liu, C.C., Feng, W., Yao, Y.: Quantum spin Hall effect in silicene and two-dimensional germanium. *Phys. Rev. Lett.* **107**, 076802 (2011)

- Liu, B., Baimova, J.A., Reddy, C.D., Law, A.W.K., Dmitriev, S.V., Wu, H., Zhou, K.: Interfacial thermal conductance of a silicene/graphene bilayer heterostructure and the effect of hydrogenation. *ACS Appl. Mater. Interfaces* **6**, 18180–18188 (2014)
- Meyer, J.C., Geim, A.K., Katsnelson, M.I., Novoselov, K.S., Booth, T.J., Roth, S.: The structure of suspended graphene sheets. *Nature* **446**, 60–63 (2007)
- Morishita, T., Spencer, M.J.S.: How silicene on Ag(111) oxidizes: microscopic mechanism of the reaction of O₂ with silicene. *Sci. Rep.* **5**, 17570 (2015)
- Nair, R.R., Ren, W., Jalil, R., Riaz, I., Kravets, V.G., Britnell, L., Blake, P., Schedin, F., Mayorov, A.S., Yuan, S., Katsnelson, M.I., Cheng, H.M., Strupinski, W., Bulusheva, L.G., Okotrub, A.V., Grigorieva, I.V., Grigorenko, A.N., Novoselov, K.S., Geim, A.K.: Fluorographene: a two-dimensional counterpart of teflon. *Small* **6**, 2877–2884 (2010)
- Novoselov, K.S., Geim, A.K., Morozov, S.V., Jiang, D., Katsnelson, M.I., Grigorieva, I.V., Dubonos, S.V., Firsov, A.A.: Two-dimensional gas of massless Dirac fermions in graphene. *Nature* **438**, 197–200 (2005)
- Özçelik, V.O., Ciraci, S.: Local reconstructions of silicene induced by adatoms. *J. Phys. Chem. C* **117**, 26305–26315 (2013)
- Özçelik, V.O., Gurel, H.H., Ciraci, S.: Self-healing of vacancy defects in single-layer graphene and silicene. *Phys. Rev. B* **88**, 045440 (2013)
- Özçelik, V.O., Cahangirov, S., Ciraci, S.: Stable single-layer honeycomblke structure of silica. *Phys. Rev. Lett.* **112**, 246803 (2014)
- Pandey, K.C.: New π -bonded chain model for si(111)-(2 \times 1) surface. *Phys. Rev. Lett.* **47**, 1913–1917 (1981)
- Perdew, J.P., Burke, K., Ernzerhof, M.: Generalized gradient approximation made simple. *Phys. Rev. Lett.* **77**, 3865–3868 (1996)
- Phillips, J.: Excitonic instabilities, vacancies, and reconstruction of covalent surfaces. *Surf. Sci.* **40**, 459–469 (1973)
- Poppendieck, T.D., Ngoc, T.C., Webb, M.B.: An electron diffraction study of the structure of silicon (100). *Surf. Sci.* **75**, 287–315 (1978)
- Qiu, J., Fu, H., Xu, Y., Oreshkin, A.I., Shao, T., Li, H., Meng, S., Chen, L., Wu, K.: Ordered and reversible hydrogenation of silicene. *Phys. Rev. Lett.* **114**, 126101 (2015)
- Sahin, H., Peeters, F.M.: Adsorption of alkali, alkaline-earth, and 3d transition metal atoms on silicene. *Phys. Rev. B* **87**, 085423 (2013)
- Sahin, H., Sivek, J., Li, S., Partoens, B., Peeters, F.M.: Stone-Wales defects in silicene: Formation, stability, and reactivity of defect sites. *Phys. Rev. B* **88**, 045434 (2013)
- Sahin, H., Leenaerts, O., Singh, S.K., Peeters, F.M.: Graphane. *Wiley Interdiscip. Rev. Comput. Mol. Sci.* **5**, 255–272 (2015)
- Schlier, R.E., Farnsworth, H.E.: Structure and adsorption characteristics of clean surfaces of germanium and silicon. *J. Chem. Phys.* **30**, 917 (1959)
- Si, C., Liu, J., Xu, Y., Wu, J., Gu, B.L., Duan, W.: Functionalized germanene as a prototype of large-gap two-dimensional topological insulators. *Phys. Rev. B* **89**, 115429 (2014)
- Sivek, J., Sahin, H., Partoens, B., Peeters, F.M.: Adsorption and absorption of boron, nitrogen, aluminum, and phosphorus on silicene: Stability and electronic and phonon properties. *Phys. Rev. B* **87**, 085444 (2013)
- Sofo, J.O., Chaudhari, A.S., Barber, G.D.: Graphane: a two-dimensional hydrocarbon. *Phys. Rev. B* **75**, 153401 (2007)
- Son, Y.W., Cohen, M.L., Louie, S.G.: Energy gaps in graphene nanoribbons. *Phys. Rev. Lett.* **97**, 216803 (2006a)
- Son, Y.W., Cohen, M.L., Louie, S.G.: Half-metallic graphene nanoribbons. *Nature* **444**, 347–349 (2006b)
- Takayanagi, K., Tanishiro, Y., Takahashi, S., Takahashi, M.: Structure analysis of Si(111)-7 \times 7 reconstructed surface by transmission electron diffraction. *Surf. Sci.* **164**, 367–392 (1985)
- Takeda, K., Shiraishi, K.: Theoretical possibility of stage corrugation in Si and Ge analogs of graphite. *Phys. Rev. B* **50**, 14916–14922 (1994)

- Tao, L., Cinquanta, E., Chiappe, D., Grazianetti, C., Fanciulli, M., Dubey, M., Molle, A., Akinwande, D.: Silicene field-effect transistors operating at room temperature. *Nat. Nanotechnol.* **10**, 227–231 (2015)
- Vogt, P., Capiod, P., Berthe, M., Resta, A., De Padova, P., Bruhn, T., Le Lay, G., Grandidier, B.: Synthesis and electrical conductivity of multilayer silicene. *Appl. Phys. Lett.* **104**, 021602 (2014)
- Wang, R., Pi, X., Ni, Z., Liu, Y., Lin, S., Xu, M., Yang, D.: Silicene oxides: formation, structures and electronic properties. *Sci. Rep.* **3** (2013)
- Wang, X., Liu, H., Tu, S.T.: First-principles study of half-fluorinated silicene sheets. *RSC Adv.* **5**, 6238–6245 (2015)
- Wei, W., Jacob, T.: Strong many-body effects in silicene-based structures. *Phys. Rev. B* **88**, 045203 (2013)
- Wierzicki, M., Barnaś, J., Swirkowicz, R.: Thermoelectric properties of silicene in the topological- and band-insulator states. *Phys. Rev. B* **91**, 165417 (2015)
- Xu, X., Zhuang, J., Du, Y., Feng, H., Zhang, N., Liu, C., Lei, T., Wang, J., Spencer, M., Morishita, T., Wang, X., Dou, S.X.: Effects of oxygen adsorption on the surface state of epitaxial silicene on Ag(111). *Sci. Rep.* **4**, 7543 (2014)
- Yang, K., Cahangirov, S., Cantarero, A., Rubio, A., D'Agosta, R.: Thermoelectric properties of atomically thin silicene and germanene nanostructures. *Phys. Rev. B* **89**, 125403 (2014)
- Zborecki, K., Wierzicki, M., Barnaś, J., Swirkowicz, R.: Thermoelectric effects in silicene nanoribbons. *Phys. Rev. B* **88**, 115404 (2013)
- Zborecki, K., Swirkowicz, R., Barnaś, J.: Spin effects in thermoelectric properties of Al- and P-doped zigzag silicene nanoribbons. *Phys. Rev. B* **89**, 165419 (2014a)
- Zborecki, K., Swirkowicz, R., Wierzicki, M., Barnas, J.: Enhanced thermoelectric efficiency in ferromagnetic silicene nanoribbons terminated with hydrogen atoms. *Phys. Chem. Chem. Phys.* **16**, 12900–12908 (2014b)
- Zhang, C.W., Yan, S.S.: First-principles study of ferromagnetism in two-dimensional silicene with hydrogenation. *J. Phys. Chem. C* **116**, 4163–4166 (2012)
- Zhang, R.Q., Chu, T.S., Cheung, H.F., Wang, N., Lee, S.T.: High reactivity of silicon suboxide clusters. *Phys. Rev. B* **64**, 113304 (2001)
- Zhang, P., Li, X., Hu, C., Wu, S., Zhu, Z.: First-principles studies of the hydrogenation effects in silicene sheets. *Phys. Lett. A* **376**, 1230–1233 (2012)
- Zheng, F.B., Zhang, C.W., Yan, S.S., Li, F.: Novel electronic and magnetic properties in N or B doped silicene nanoribbons. *J. Mater. Chem. C* **1**, 2735–2743 (2013)
- Zhang, W.B., Song, Z.B., Dou, L.M.: The tunable electronic structure and mechanical properties of halogenated silicene: a first-principles study. *J. Mater. Chem. C* **3**, 3087–3094 (2015)
- Zólyomi, V.Z., Wallbank, J.R., Fal'ko, V.I.: Silicene and germanane: tight-binding and first-principles studies. *2D Materials* **1**, 011005 (2014)

Introduction to the Physics of Silicene and other 2D
Materials

Cahangirov, S.; Sahin, H.; Le Lay, G.; Rubio, A.

2017, X, 96 p. 52 illus., 51 illus. in color., Softcover

ISBN: 978-3-319-46570-8